Low-Defect, Purified, Narrowly (*n*,*m*)-Dispersed Single-Walled Carbon Nanotubes Grown from Cobalt-Incorporated MCM-41

Yuan Chen,[†,‡,*] Li Wei,[‡] Bo Wang,[‡] Sangyun Lim,[†] Dragos Ciuparu,[†,§] Ming Zheng,[⊥] Jia Chen,[#] Codruta Zoican,[†] Yanhui Yang,[†,‡] Gary L. Haller,[†] and Lisa D. Pfefferle[†]

[†]Department of Chemical Engineering, Yale University, New Haven, Connecticut 06520, [‡]School of Chemical and Biomedical Engineering, Nanyang Technological University, 637722, Singapore, [§]Petroleum Processing and Petrochemical Engineering Department, Petroleum-Gas University of Ploiesti, Ploiesti 100680, Romania, [⊥]DuPont Central Research and Development, Experimental Station, Wilmington, Delaware 19880, and [#]IBM T. J. Watson Research Center, Yorktown Heights, New York 10598

ABSTRACT A mild, four-step purification procedure using NaOH reflux, HCl wash, and oxidation by 4 mol % molecular oxygen at 500 °C was developed to purify single-walled carbon nanotubes (SWCNTs) with narrow semiconducting (*n*,*m*) distribution produced from cobalt-incorporated MCM-41 (Co-MCM-41) in order to obtain bulk low-defect-density nanotubes. Three key features of Co-MCM-41 allow this mild purification technique: (1) ultrathin silica walls *versus* dense silica or other crystalline oxide supports are soluble in dilute NaOH aqueous solution, which avoids the damage to SWCNTs usually caused by using HF treatment to remove catalytic supports; (2) the small metallic particles are easily dissolved in HCl, a significantly milder chemical treatment compared to HF or HNO_3; (3) the high selectivity to SWCNTs with negligible multiwalled carbon nanotubes or graphite, which facilitates the removal of undesired carbon species by selective oxidation. The effectiveness of this purification procedure was evaluated by high-resolution transmission electron microscopy, scanning electron microscopy, Raman, UV–vis—NIR, and fluorescence spectroscopy, solution redox chemistry on fractionated (6,5) tubes, and SWCNT-based field effect transistor device performance. The results demonstrate that Co-MCM-41 catalyst not only provides tubes with narrow semiconducting (*n*,*m*) distribution but also allows a mild purification procedure and, therefore, produces SWCNTs with fewer defects.

KEYWORDS: single-walled carbon nanotubes · purification · chirality · defect · MCM-41

The unique electrical and mechanical properties of single-walled carbon nanotubes (SWCNTs) make them ideal candidates for novel molecular devices.[1] Each (*n*,*m*) nanotube can be considered to be a distinct molecule with a unique structure because the indices *n* and *m* specify the unique manner in which a single layer of graphite is rolled up seamlessly to form the carbon nanotube.[2] Applications of SWCNTs in nanoscale electronic devices require large-scale synthesis of low-defect-level tubes at specified (*n*,*m*) chirality. This requirement has not been fulfilled by current SWCNT production techniques and remains one of the central challenges in SWCNT research. All current SWCNT production techniques inevitably result in significant contamination. SWCNTs produced by chemical vapor deposition (CVD) are contaminated with transition metal residues and amorphous silica or other supports, MgO, *etc*. SWCNT growth also generates a great amount of carbonaceous impurities, such as amorphous carbon, carbon nanoparticles, multiwalled carbon nanotubes (MWCNTs), and graphite. Physical and chemical properties of SWCNTs are strongly affected by these impurities. Various techniques have been explored to purify SWCNTs.[3–11] A hierarchical flowchart for SWCNT purification was proposed by Haddon *et al*.[8] However, crystalline or dense amorphous oxide supports are difficult to remove without using strong acids such as HF. Purification by HF or HNO_3, commonly used in many purification procedures,[12–15] introduces defect sites in the nanotubes, which affect their performance in electronic applications. Molecular oxygen oxidation methods[16,17] cannot remove MWCNTs and graphite because they have higher oxidation temperatures than that of SWCNTs. The metallic alloys or metallic carbides such as Mo carbide[18] are difficult to remove without introducing defects to SWCNTs by HF treatment. Although applying strong tip sonication to disperse SWCNTs in a solution followed by high-speed centrifugation can produce a small amount of SWCNTs for research, the process has a low purified tube yield. A large fraction of samples is discarded in centrifuge residues. It is also

*Address correspondence to chenyuan@ntu.edu.sg.

Received for review July 17, 2007 and accepted October 25, 2007.

Published online November 30, 2007.
10.1021/nn700106c CCC: $37.00

difficult to scale up the sonication plus high-speed centrifugation process for bulk production.

We have developed a catalyst system that incorporates single metal cobalt into the pore wall of MCM-41 mesoporous molecular sieves by isomorphous substitution of silicon. It can produce SWCNTs within ±0.05 nm diameter distribution.[19–22] A recent comprehensive analysis shows that they have the narrowest (*n*,*m*) distribution for semiconducting tubes reported so far.[23] SWCNTs produced by Co-MCM-41 are not only uniform in diameter but also contain <10% amorphous carbon and graphite and no detectable MWCNTs.[21,22] Moreover, the amorphous silica-based catalyst (with ultrathin silica wall at about 1 nm)[24] is soluble in dilute NaOH aqueous solutions. A considerably less aggressive chemical treatment for SWCNTs is required compared to the use of HF treatment to dissolve dense silica or other crystalline oxide supports. The small metallic particles produced are easily dissolved in HCl, a significantly milder chemical treatment compared to use of HF or HNO_3.

In this study, we took advantages of these key features and developed a four-step procedure to purify SWCNTs produced from Co-MCM-41. The effectiveness of this purification procedure was evaluated by Raman, UV–vis–NIR, and florescence spectroscopy, high-resolution transmission electron microscopy (HR-TEM), and scanning electron microscopy (SEM). Moreover, the purified nanotubes were separated by the DNA-assisted method to obtain single chirality enriched samples.[25,26] The solution redox titration analysis of the (6,5)-enriched fraction was studied.[27] A SWCNT-based field effect transistor (FET) was fabricated from purified tubes to demonstrate their potential for electronic device applications, using a method described previously.[28]

RESULTS AND DISCUSSION

Four-Step Purification Procedure. Three issues need to be addressed in the purification of SWCNTs synthesized from Co-MCM-41: removal of the silica that comprises the MCM-41 matrix, cobalt metal residues, and amorphous carbon. HF treatment is commonly used to dissolve silica. Gas-phase oxidation based on the idea of selective oxidation may be used to remove amorphous carbon, and various acid washing methods may be used to eliminate metallic residues. Here we first discuss procedures we used in each purification step and then rationalize the sequence of the multiple-step purification approach.

The first step was the removal of MCM-41, an amorphous form of silica of 1 nm thickness. HF is widely used to remove dense amorphous silica, although it obviously introduces defect sites on SWCNTs.[14,15] Two methods of using HF to remove MCM-41 from as-synthesized SWCNTs were tested in this study. One was to sonicate as-synthesized SWCNTs in 48 wt % HF for 2 h in a bath sonicator, followed by filtering diluted HF solution (<0.1 wt %), which contains the SWCNTs. The other was to sonicate the SWCNTs in a dilute 10 wt % HF solution for 8 h, followed by filtration in an attempt to minimize the damage to SWCNTs caused by HF.

Raman spectroscopy was used to evaluate the different purification procedures. Three features in Raman spectra of SWCNTs of interest to this work are the radial breathing mode (RBM) below 400 cm^{-1}, the disorder-induced band (D) centered near 1300 cm^{-1}, and the graphite-like band complex (G) located between 1580 and 1600 cm^{-1}. The G band of SWCNTs has multipeak features for semiconducting and metallic tubes because of the symmetry breaking of the tangential vibration when the graphite sheet is rolled.[29] Usually, the semiconducting tube line can be fitted with a Lorentzian line shape, while the metallic feature is usually fit using a Breit–Wigner–Fano (BWF) line shape.[30] The D band is used for characterization of defective or functionalized sites, but no systematic study has been carried out to correlate the presence of the D band with specific defect sites (such as heteroatoms, vacancies, heptagon–pentagon pairs, kinks, the presence of impurities, *etc.*). [29] The Raman scattering intensity (especially that of RBM peaks) becomes much higher when the excitation energy ($E_{laser} = h\nu_0$) matches allowed electronic transitions of SWCNTs during resonance Raman scatterings.[29]

Raman spectroscopy studies (not shown) indicated that both HF treatment methods greatly increased the intensity and width of the D band in Raman spectra of purified SWCNTs, suggesting that SWCNTs were damaged by these HF treatments. Although the defects caused by HF treatments may prove useful for SWCNT functionalization, for better FET performance, SWCNTs without significant defects are desired.

A milder treatment using 1 M NaOH to remove MCM-41 silica was selected. About 1 g of as-synthesized SWCNTs was mixed with 500 mL of 1 M NaOH solution (20 g of NaOH, 250 mL of H_2O, and 250 mL of ethanol) and refluxed for 1 h, followed by filtration. The carbon film collected on the 0.4-μm pore nylon membrane filter was redispersed in a new batch of 500 mL of 1 M NaOH solution. After the second 1 h reflux followed by filtration, the silica was successfully removed, as observed in the TEM images shown in Figure 1. Figure 1C,D (samples after silica removal by NaOH) show the presence of cobalt clusters. The cobalt concentration in SWCNT samples after the silica MCM-41 removal is very high (up to 23.5 wt %). Cobalt clusters in intimate contact with SWCNTs are known to act as oxidation catalysts in the presence of oxygen, lowering the oxidation temperature of SWCNTs.[31] This affects the efficiency of the amorphous carbon removal process by selective oxidation. Indeed, SWCNTs attached with cobalt residues were destroyed in the presence of oxygen,

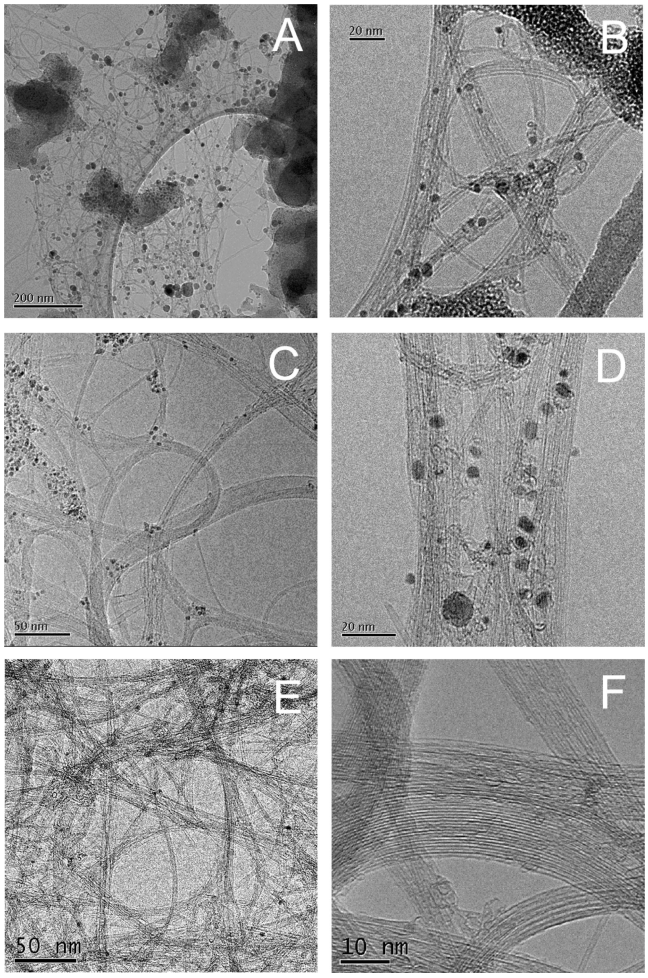

Figure 1. TEM images showing the structure of SWCNTs: (A,B) as-synthesized SWCNT bundles with Co-MCM-41 catalysts, (C,D) SWCNT bundles with cobalt clusters after silica removal, and (E,F) SWCNT bundles purified after the second HCl wash.

even at 250 °C. Therefore, the second step of our purification procedure was to eliminate cobalt residues.

H_2SO_4, HNO_3, HF, and HCl have been used by researchers to remove metallic residues.[12–15] Usually, strong oxidative acids such as H_2SO_4, HNO_3, and HF are required for large metal particles covered by thick graphite carbon layers, and they introduce many defect sites and carboxyl groups on side walls of SWCNTs after acid washes.[12–15] Because Co-MCM-41 produces smaller metal particles,[24] we expected that a less oxidative acid, HCl, could be used. After the first HCl treatment, cobalt clusters originally exposed to the atmosphere, which could act as catalysts for SWCNT oxidation under oxygen treatment, were eliminated. An oxidation treatment is then possible to remove the amorphous carbon species deposited during SWCNT synthesis and minimize the loss of valuable nanotubes. However, other Co clusters covered by thick layers of carbon, either amorphous or graphite, cannot be removed in the first HCl treatment. Carbon layers covering cobalt clusters must be removed in order to make the clusters accessible to HCl.

In order to optimize the selective oxidation treatment, we studied the efficiency of using 4% O_2 in He to remove amorphous carbon. Many gas-phase oxidation methods have been explored by researchers.[8,16] The key problem, as pointed out by Haddon *et al.*,[8] is that the metal particles catalyze low-temperature oxidation of carbon indiscriminately, resulting in destruction of SWCNTs. About 50 mg of Co-MCM-41 samples containing SWCNTs was loaded into a quartz tube placed inside a tubular furnace. Helium was flowed through the tube, and the temperature of the furnace was ramped up to the desired temperature (from 250 to 700 °C). Then, 4% O_2 balanced to 1 atm by He was introduced for 30 min at a flow rate of 50 sccm. After oxidation, the samples were cooled in He to room temperature and analyzed by Raman spectroscopy. Figure 2A shows Raman spectra of as-synthesized SWCNT samples after oxidation at different temperatures.

We initially intended to use thermal gravimetric analysis (TGA) to quantify different carbon species. However, TGA is not successful due to the interference of cobalt residues attached to nanotubes.[31] To assess the efficiency of amorphous carbon removal by oxidation, two quality indices were calculated from the Raman spectra: RBM/(D+G) and D/G. Researchers[32,33] have proposed that the intensity ratio of D and G bands (D/G) is related to the sp^2 carbon cluster sizes in the graphite sheet and is nearly proportional to defect site density. However, an accurate quantitative method to determine the concentration and the quality of SWCNT from Raman spectra is still not available. The resonance effects on the Raman spectra make it hard to calibrate the intensity of RBM with the concentration of SWCNT in samples. Moreover, the relationship between the D band and specific defect types is still unclear, and defect components could be either resonant or nonresonant. In the present study, all SWCNT samples had about the same SWCNT chirality distribution (shown in fluorescence and absorption spectroscopy analysis) and the same amount and type of defects before the oxidation treatment. Therefore, any change in SWCNT structure and defects caused by oxidation can be directly correlated with the changes in the intensities of RBM and D bands. Thus, the ratio between the integrated areas of the RBM and the sum of D and G bands (RBM/(D+G)) were used to evaluate the amount of SWCNTs remaining in the sample after oxidation. The area ratio between the D and G bands (D/G) was used as an indication for the amount of amorphous carbon in the sample.

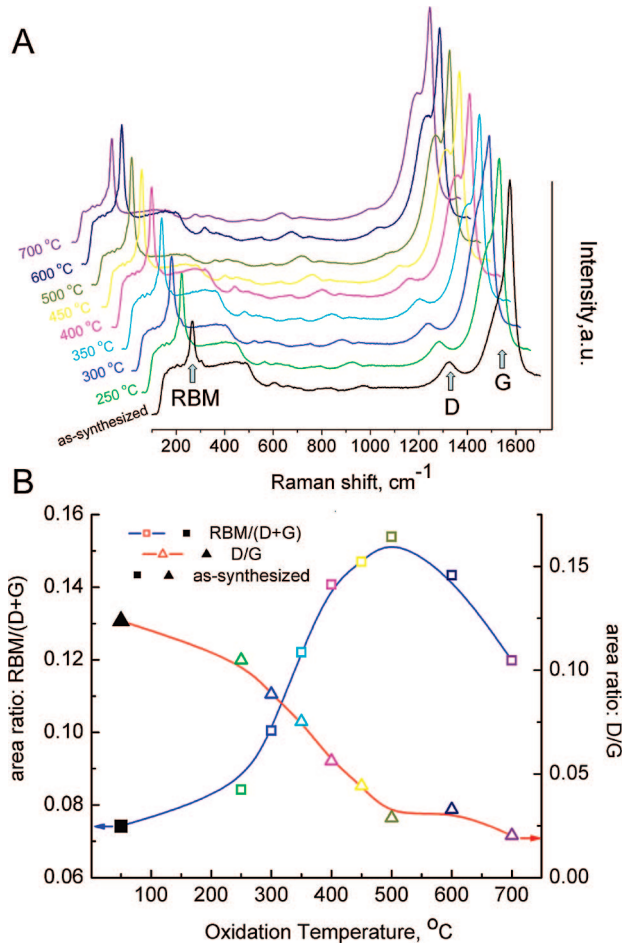

Figure 2. (A) Raman spectra of SWCNTs on Co-MCM-41 after oxidation by 4% O_2 for 30 min at different temperatures. (B) Correlation between SWCNT quality indices and oxidation temperature.

The correlation between the two quality indices and the oxidation temperatures is shown in Figure 2B. The RBM/(D+G) ratio increased with the oxidation temperature from 250 to 500 °C. At higher oxidation temperatures, the RBM/(D+G) ratio began to decrease as the oxidation temperature increased. On the other hand, the D/G ratio continually decreased at increasing oxidation temperatures below 500 °C. However, there was a slight increase in D/G ratio as the oxidation temperature increased above 500 °C, followed by decreases again at 700 °C. The change can be explained on the basis of the different oxidation temperatures for different carbon species. Nanotubes are harder to be oxidized than amorphous carbon. At temperatures below 250 °C, only amorphous carbon was removed, and SWCNTs were not attacked. The RBM intensity, reflective of SWCNTs, did not change, while the D band, correlated with amorphous carbon, decreased. The G band, correlated with ordered carbon in SWCNTs and graphite, also remained unchanged after oxidation at low temperatures. Thus, there was an increase of RBM/(D+G) ratio and a decrease in D/G ratio in Figure 2B. When the temperature was higher than 500 °C, oxidation of SWCNTs resulted in the decrease of the RBM/(D+G) ratio. The oxidation of SWCNTs could introduce defects on the side wall or convert them completely to CO_2. These defects and/or production of amorphous carbon would increase the D/G ratio. At 700 °C, both SWCNTs and amorphous carbon were oxidized quickly. However, graphite is not attacked until around 900 °C.[34] The fast removal of amorphous carbon causes the D/G ratio to decrease again. Considering the balance between amorphous carbon removal and oxidative damage to SWCNTs, oxidation in 4% O_2 was an effective treatment for cleaning amorphous carbon from our SWCNT samples at temperatures between 400 and 500 °C.

Since oxidation in 4% O_2 at 500 °C was shown to remove most of the amorphous carbon, as indicated by the Raman spectrum in Figure 2, this oxidative treatment was applied after MCM-41 and Co removal. Because each oxidation treatment unavoidably damages some tubes, a single oxidation step is preferred to minimize SWCNT damages. A recent X-ray absorption spectroscopy study on the mechanism of cobalt clusters growth on Co-MCM-41 catalysts[35,36] indicated that the amorphous carbon most likely forms on large metallic cobalt species resulting from the fast reduction and migration of Co^{3+} and surface Co^{2+} species in the catalyst. After oxidation in 4% O_2, cobalt clusters covered by amorphous carbon are exposed to the atmosphere, and thus should be easily removed by a second HCl treatment.

Therefore, the complete purification process developed in this study consists of a four-step procedure: (1) as-synthesized SWCNTs are refluxed in 1 M NaOH solution twice for 1 h each to remove silica, followed by filtration; (2) the carbon products collected on the filter are then dispersed in 37% HCl solution and refluxed for 8 h, followed by filtration; (3) the carbon collected from filter is then oxidized by 4% O_2 at 500 °C for 30 min to remove the amorphous carbon covering the metallic cobalt clusters; and (4) the products after oxidation are refluxed in 37% HCl solution for 8 h to remove cobalt residues exposed after the oxidation treatment.

Evaluation of Purification Procedure. As-synthesized SWCNTs and samples after each purification step were characterized by TEM, SEM, Raman, UV–vis–NIR absorption, and fluorescence spectroscopy to evaluate the performance of each purification step. The TEM images in Figure 1 show that the silica is completely removed by NaOH wash. After silica removal, SWCNTs were contaminated by cobalt clusters. Most of the cobalt residues were removed after the double HCl wash. SEM images in Figure 3 were taken directly from carbon films coated on filters after different purification steps. They are consistent with the TEM images. Figure 3A,D (samples after silica removal by NaOH) show many white spots, indicating the presence of cobalt clusters (as confirmed by elemental analysis). After the HCl treatment, most of white spots disappeared, as shown in Figure 3C,E. Energy-dispersive spectrometry (EDS) data

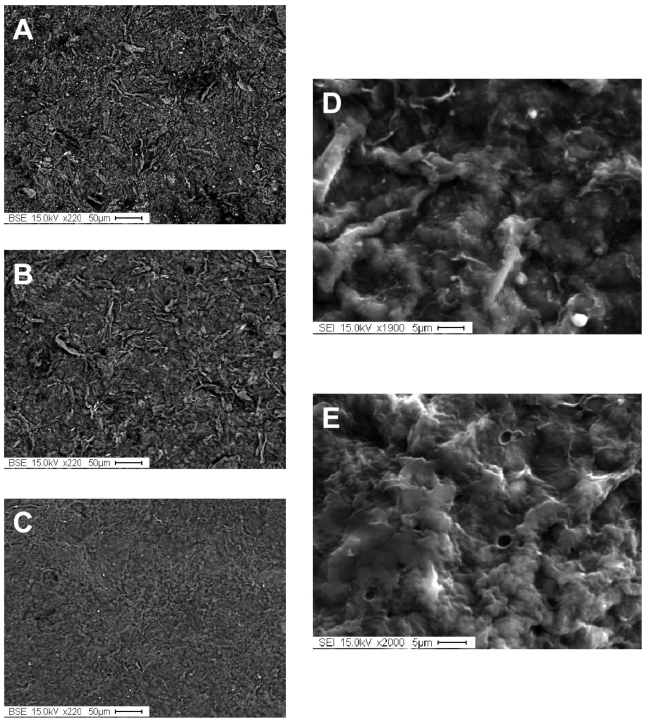

Figure 3. SEM images of SWCNT samples during purification: (A) after silica removal by NaOH, (B) after the first HCl wash, and (C) after the second HCl wash. (D,E) Higher resolution images of (A) and (C), respectively.

from SEM images were used for both qualitative elemental identification and semiquantitative composition estimates. The results of the compositional analysis are shown in the Supporting Information, Figure S1. After silica removal, the sample contained as much as 23.5 wt % cobalt residues. After the first HCl wash, the cobalt concentration only dropped to 18.4 wt %, indicating that most of the cobalt clusters were covered by carbon and not accessible to HCl. After oxidation and the second HCl wash, the cobalt concentration dropped to 2.2 wt % or 0.5 atom %, indicating that oxidative removal of the carbon covering cobalt clusters was effective and that those cobalt clusters exposed were removed by the second HCl wash. The remaining 2.2 wt % cobalt consists most likely of cobalt particles covered with graphite, which cannot be eliminated by selective oxidation followed by HCl treatment and require other purification methods. The silicon concentration was approximately 0.2 wt %, showing that silica was almost completely removed. EDS indicated that the final purified SWCNT samples consisted of 88.1 wt % of carbon and about 6.7 wt % oxygen. Oxygen signals most likely originate from hydroxyl or carboxyl groups introduced to the SWCNT surface during purification and from the water adsorbed in the sample.

Figure 4 shows Raman spectra recorded after each purification step. Purified carbon films on filter papers show more intense RBM peaks compared with those from as-synthesized catalyst powers. (7,5) tubes may contribute significantly to the RBM peak shown in Figure 4 at 266 cm^{-1}, because they are the most abundant semiconducting tubes identified in fluorescence spectroscopy. The Raman excitation energy (at 532 nm) is also close to their allowed electronic transitions. Minor changes were observed in Raman spectra recorded after each subsequent purification treatment, which demonstrate that the final purification procedure did not produce significant defects in the SWCNT (no significant D band increase) and that the SWCNT structure was well preserved (insignificant RBM changes). The intensity of BWF line shape (G band) changes among samples as shown in Figure 4. The BWF component was initially found to be intrinsic to individual metallic SWCNTs.[37] It also changes due to bundling/debundling effects.[38] For the four-step purification procedure, tubes are all bundled. Neither metallic nor semiconducting selectivity is found in neither UV–vis−NIR nor florescence spectroscopy. We reason that the change of BWF components in Figure 4 is due to the electron donation and withdrawal from metallic SWCNTs during NaOH and HCl treatments. Similar phenomena have been reported previously. [39]

There are still no standard methods to accurately evaluate the purity of SWCNT samples. Haddon *et al.*[40] proposed solution-phase NIR spectroscopy to quantitatively compare the purity of bulk SWCNT materials. Several issues, however, complicate this method. First, there are no defect-free SWCNT reference samples available. This means that NIR cannot give an absolute determination of SWCNT purity, but rather a relative comparison among samples. Second, a more serious problem is that the interband electronic transitions of SWCNTs change drastically following chemical functionalization of SWCNTs that can occur during dispersion in solutions,[41] oxidation by acids or doping by halogens, and even the physical environment such as a high pressure.[42] Although the S_{22} tran-

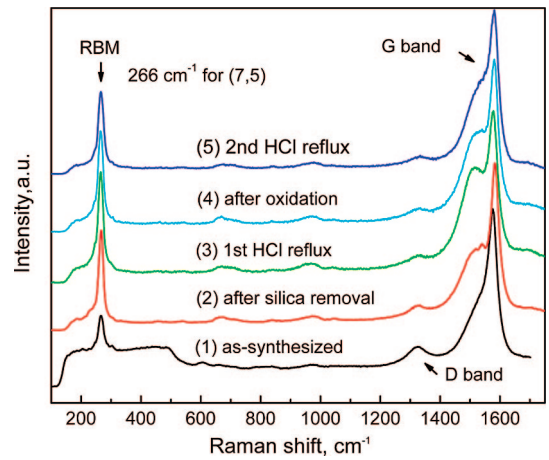

Figure 4. Raman spectra of SWCNT samples after different purification steps.

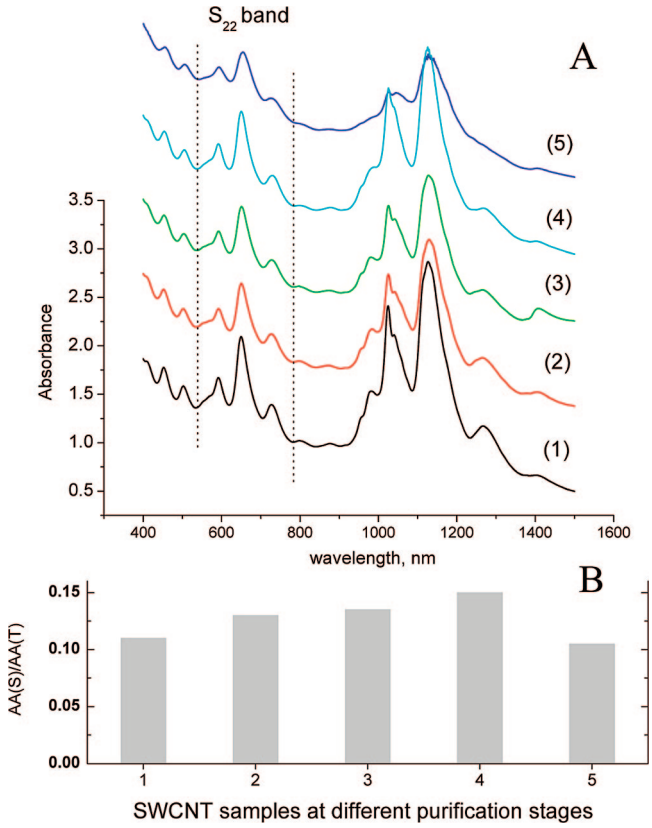

Figure 5. (A) Solution-phase UV–vis–NIR spectra for SWCNT samples at different purification stages. (B) Purity index (AA(S)/AA(T)) of SWCNT samples. Labels (1)–(5) correspond to the sample numbers in Figure 4.

sition of SWCNT may be less susceptible to incidental doping,[40] the effect of purification procedures involving oxidation by acids and dispersion in solutions on the S_{22} transition is still unclear. Clarifying these issues is beyond the scope of this study. To assess defect levels, we simply adopted a modified method suggested by Haddon *et al.*,[40] utilizing the S_{22} interband transition for purity evaluation. UV–vis–NIR spectra of SWCNT samples at different purification stages are shown in Figure 5A. The region between two dotted lines is the S_{22} interband transition for tubes identified in SWCNTs produced on Co-MCM-41. AA(T) is the total area of the S_{22} band including SWCNTs and carbonaceous impurity contributions. AA(S) is the area of the S_{22} spectral band after linear baseline correction. [40] A purity index ratio AA(S)/AA(T) from the S_{22} bands of SWCNT samples is shown in Figure 5B. The as-synthesized SWCNTs have an index of 0.11, compared with SWCNTs having an index ratio of 0.057 and 0.095 in ref 43. After silica removal, HCl wash, and oxygen oxidation, the purity index increases to 0.15, suggesting that some carbonaceous impurities have been removed. After the second HCl wash, the purity drops back to 0.105. This change may result from defect sites introduced in the HCl wash. However, the effect of acid wash on the S_{22} interband transition also cannot be ruled out. More information about the defect level in our samples was studied in solution redox reactions, as discussed below.

One of the key advantages of SWCNTs produced from Co-MCM-41 is that they have a narrow semiconducting (*n*,*m*) distribution. [23] This provides a good starting material for separating SWCNTs by chirality and various electronic device fabrication. We applied fluorescence spectroscopy to monitor the chiral distribution of semiconducting tubes during the purification procedure. Figure 6 illustrates the two-dimensional fluorescence–excitation map for the aqueous dispersion of SWCNT samples at different purification stages with excitation scanned from 300 to 850 nm and emission collected from 900 to 1600 nm. The resonance behavior

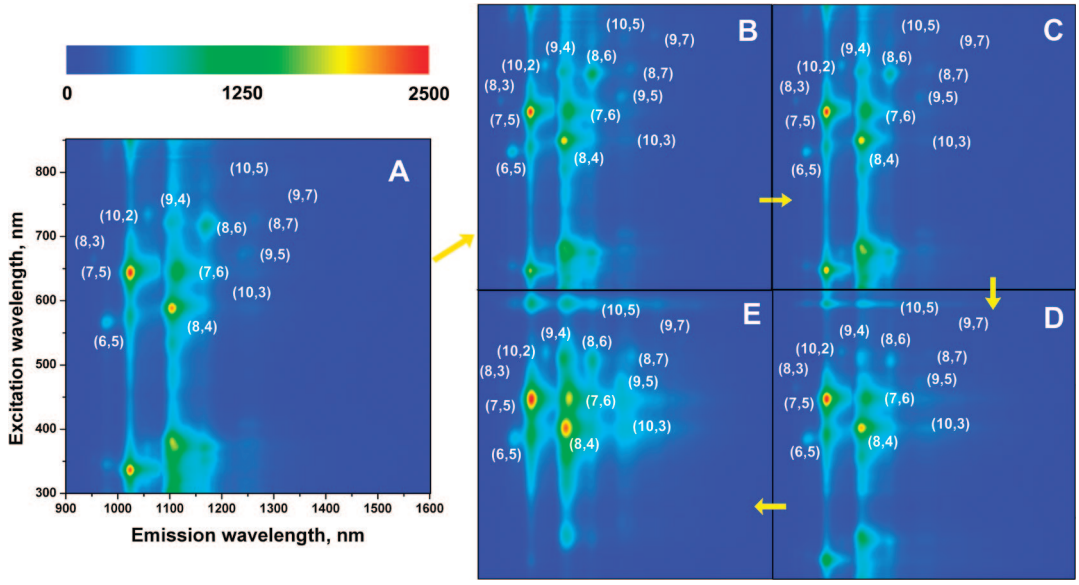

Figure 6. Fluorescence intensity map as a function of excitation and emission wavelength for SDBS-micellarized SWCNTs in D_2O at different purification stages: (A) as-synthesized, (B) after silica removal by NaOH, (C) after the first HCl wash, (D) after oxidation, and (E) after the second HCl wash

of both excitation and emission events results in spikes corresponding to the transition pair from individual (*n*,*m*) SWCNTs. (*n*,*m*) assignment on the map is based on previous experimental and theoretical studies.[44,45] Figure 6 shows that narrow chirality distribution SWCNTs were produced on Co-MCM-41. Five spectra were recorded at the same intensity scale, and the similar spectral patterns also indicate that the chirality distribution is not altered during our purification steps.

Overall, the four-step purification procedure used in this study provides purified SWCNTs with a narrow diameter distribution for applications where this is required. It is the special properties of the Co-MCM-41 catalyst that make this purification procedure feasible. First, MCM-41 is composed of amorphous silica, and the walls are very thin, about 1 nm. [24] Compared with dense silica or other crystalline oxide supports used in many other SWCNT synthesis methods, MCM-41 silica is much easier to remove by milder treatments than HF treatment. This helps to minimize the defects produced during HF treatment. Second, Co-MCM-41 produces significantly fewer large metallic particles, as discussed in our previous report.[24] Small metallic clusters in Co-MCM-41 minimize the production of MWCNTs and graphite, which was confirmed by TGA of the as-synthesized samples.[34] MWCNTs and graphite cannot be removed easily from SWCNTs by selective oxidation. Third, small cobalt clusters can be removed by milder acid treatments. The metallic alloys or metallic carbides are difficult to remove without damaging SWCNTs through strong oxidative acid treatments.

Chiral Separation and Redox Titration Analysis. Separation of SWCNTs by chirality to obtain SWCNT samples with a single chirality type is crucial for many potential applications and fundamental studies that require defined SWCNT structures. A DNA-assisted separation method may solve this problem.[25,26] It should be simpler to obtain a single (*n*,*m*)-type tube from a starting material with a narrow chirality distribution, which contains limited tube types, than from samples having tubes of many different chiralities. SWCNTs grown on Co-MCM-41 show a narrow chirality distribution, as confirmed by fluorescence measurements. The purified SWCNT samples were processed in an attempt to separate tubes by chirality.

The DNA separation method is based on the fact that a particular single-stranded DNA $(d(GT)_n$, $n = 10-45$, G is guanine, T is thymine) self-assembles into an ordered supramolecular structure around individual SWCNTs. For metallic tubes, the discrete negative charges on the DNA create an electrostatic field along the tube axis, which induces a positive screening image charge in the nanotube. As a result, the net linear charge density of the DNA−SWCNT hybrid is reduced from that of the DNA wrap alone. For semiconducting tubes, the lower polarizability of the nanotube, compared with that of the surrounding water, results in an increase in the effective linear charge density of the DNA−SWCNT hybrid relative to that of the DNA wrap alone, based on an image charge analysis for adjacent dielectrics. This fundamental difference provides a way to separate them by using ion-exchange chromatography. SWCNTs with different chiralities can be enriched in different fractions of a solvent by passing through the ion-exchange column, because of their different interaction with the chromatography column.

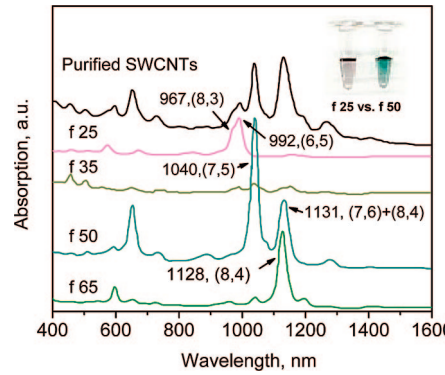

Figure 7. UV–vis−NIR spectra demonstrating the separation of SWCNTs from Co-MCM-41 by chirality using a DNA-assisted method. The trace labeled as "Purified SWCNTs" was the unfractionated starting SWCNT solution. Traces labeled f25, f35, f50, and f65 were from different fractions of anion-exchange chromatography. The inset shows an image of fractions f25 and f50.

Purified SWCNTs were processed as described in the Methods section. Different fractions from the anion-exchange chromatographic separation were analyzed by UV–vis−NIR spectroscopy, as shown in Figure 7. Based on the empirical Kataura plot developed by Weisman *et al.*,[46] fraction f25 had two major pairs of (S_{11},S_{22}) peaks. They were (6,5) at (992 nm, 574 nm) and (8,3) at (967 nm, 674 nm). Fraction f35 had two strong peaks from metallic tubes at 458 and 507 nm. The strongest (S_{11},S_{22}) pair in fraction f50, at (1040 nm, 653 nm), was from (7,5). The peak at 1131 nm was probably from an overlap of S_{11} from (7,6) and (8,4) with corresponding S_{22} at 731 and 597 nm, respectively. Fraction f65 was enriched with a single chirality of (8,4) at (1128 nm, 597 nm). Intensity comparison suggested that the major species in SWCNTs produced on Co-MCM-41 were (7,5), (7,6), and (8,4).

Redox titration analysis of fractionated SWCNT was used to estimate their defect levels.[27] For optically the same amount of (6,5) tubes from Co-MCM-41 and commercial available CoMoCAT SWCNTs, (6,5) is the only chiral type that we can purify from both samples at the present time; we found that the former has ~20% less reducing equivalent than the latter. Since the number of reducing equivalents is determined by the number of valence electrons, the redox titration result indicates that Co-MCM-41 SWCNTs yield higher optical density per valence electron. This result can be interpreted qualitatively using the simple classical oscillator model. For a given oscillator, its imperfection (or defect level) is

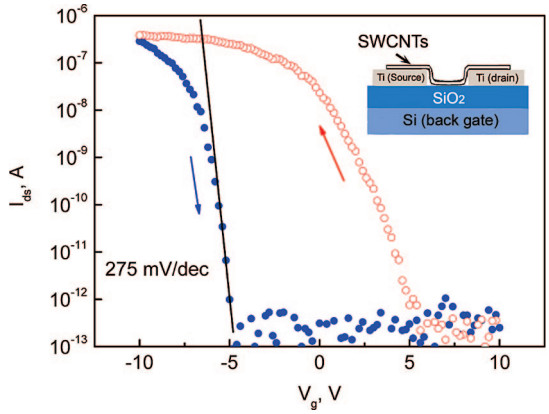

Figure 8. Transfer characteristics of a SWCNT-FET. The open and solid curves are forward and backward voltage scans, respectively. The bias was 0.5 V. Inset shows the schematic cross section of the SWCNT-FET device.

described by a quality factor *Q*, which determines the amplitude of oscillation. The higher the *Q* value, the higher the oscillation amplitude. We treat defects as imperfections that lower the *Q* value. A change in SWCNT redox potential, which is determined by the electronic structure, may affect redox titration. Since in both UV–vis−NIR absorption and fluorescence measurements, no noticeable changes in the E_{11} and E_{22} position of the tubes in our samples were observed, we reason that the electronic structure and redox potential of tubes are not different from those synthesized/purified by others. On the basis of this model,[27] it suggests that valence electrons in the Co-MCM-41 SWCNT have higher *Q* values, and therefore the material itself has lower defect levels.

Fabrication of SWCNT-Based FET. The fabrication of SWCNT-based field-effect transistors (SWCNT-FETs) is a promising application of SWCNTs. Purified SWCNT samples from Co-MCM-41 after the second HCl wash were tested for preliminary device demonstration. SWCNTs were dispersed by sonication in dichloroethane and then spread on a substrate with predefined electrodes. The inset in Figure 8 shows the schematic cross section of the SWCNT-FET. The device has titanium source and drain electrodes separated by 300 nm on top of 10 nm SiO_2, and a Si backgate.[28] The typical device transfer characteristics (I_{ds} *vs* V_g) at V_{ds} = 0.5 V, measured under ambient conditions at room temperature, are shown in Figure 8. The open and solid curves represent forward and backward voltage scans, respectively. It demonstrates a high subthreshold swing $S = dV_g/d(\log I_d)$ at 275 mV/dec. The current I_{ds} is 0.38 μA, which is significantly improved compared with those obtained with previous devices.[47] The hysteresis shown in Figure 8 can be attributed to the charge trapping by water molecules around the nanotubes, as suggested by Kim *et al.*[48] Unlike conventional transistors made from bulk materials, SWCNT-FETs are sensitive to their environment.[28] Defects in SWCNTs compromise their performance. Large-scale production of high-purity SWCNTs without defects is desirable. This preliminary result suggests that SWCNTs synthesized using Co-MCM-41 and purified as described here with high purity and minimized defects show potential for electronic device applications.

CONCLUSION

A four-step purification procedure using 1 M NaOH reflux, 37 mol % HCl wash, and oxidation by 4 mol % molecular oxygen at 500 °C was developed to purify SWCNTs from Co-MCM-41. SWCNTs have a narrow diameter distribution, and the major semiconducting species are (7,5), (7,6), and (8,4). Special properties of the Co-MCM-41 catalyst enable this purification procedure. Unlike dense silica or other crystalline oxide supports, amorphous silica of 1 nm thickness comprising the wall of MCM-41 can be dissolved in a mild NaOH reflux, which avoids the damage of SWCNTs usually caused by HF treatment. Small metallic clusters produced in Co-MCM-41 minimize the production of MWCNTs and graphite. Cobalt clusters can be removed by a mild HCl treatment combined with selective 4 mol % molecular oxygen oxidation at 500 °C without damaging SWCNTs through strong oxidative acid treatments. Purified SWCNTs were separated into single chirality-enriched fractions using a DNA-assisted method. The redox test performed on (6,5) tubes suggests a low defect level. SWCNT-FETs fabricated using purified tubes indicate that the SWCNT device has a high subthreshold swing at 275 mV/dec and a current I_{ds} at 0.38 μA, exhibiting potential for electronic device applications.

METHODS

The Co-MCM-41 catalyst was prepared following the procedure described previously.[19] The reducibility of cobalt in Co-MCM-41 was found to be highly sensitive to synthesis parameters (such as pore size of MCM-41, pH, and silica source used).[24,49] One optimized synthesis condition was used to produce C16-Co-MCM-41 (C16 chain surfactants were used) with 1 wt % cobalt loading (analyzed by inductively coupled plasma (ICP) at Galbraith Laboratories, Inc.), showing a high structural order with an average pore diameter of 2.85 and 0.1 nm full width at half-maximum pore size distribution (by BJF method[50]). Cobalt reduction showed a single peak in the temperature-programmed reduction (TPR) experiment, with the temperature of maximum reduction rate at 808 °C.[24]

The starting SWCNT samples were obtained on Co-MCM-41 by an optimized synthesis method described in previous publications.[21,22] For a typical batch, 200 mg of fresh Co-MCM-41 was heated to 500 °C and reduced isothermally for 30 min in flowing hydrogen at 1 atm. After prereduction, the catalyst was purged with argon and then heated to 800 °C in flowing argon. CO (99.5% from Airgas) was introduced at 6 atm to grow SWCNT for 1 h. The CO feed was first passed through a carbonyl trap to eliminate iron pentacarbonyl originating from the CO container.

Five synthesis batches, weighing about 1 g, of Co-MCM-41 loaded with carbon were mixed. The total carbon loading on

the catalyst is about 1.25 wt % from 1 wt % Co loading catalyst. The MCM-41 template, cobalt clusters, and carbonaceous impurities were removed by a sequence of purification procedures. Fifteen weight percent of total carbon products were lost during purification steps due to the oxidation of amorphous carbon and residues left on filter papers. On average, we obtained 10 mg of purified SWCNTs from 1 g of catalysts. Details of each purification procedure are given in the Results and Discussion section. After each purification step, SWCNTs were characterized by TEM, SEM, Raman, UV–vis−NIR, and fluorescence spectroscopy.

High-resolution TEM images of SWCNTs were collected on a Tecnai F20 200 kV microscope from Philips. The solid samples were dispersed in ethanol by sonication, and 0.05 mL of this suspension was dropped on a copper mesh coated with an amorphous holey carbon film. The ethanol evaporated prior to the TEM analysis.

Experiments in this work showed that purified SWCNTs had enough conductivity to avoid electrical charge buildup; thus, they were not coated with gold. SEM images of purified SWCNTs were obtained using EDS collected with an EDAX Phoenix Pro EDS/imaging system (EDAX, Mahwah, NJ) on a JEOL JXA-8600 electron microprobe (JEOL, Peabody, MA). EDS data were used for both qualitative element identification and semiquantitative compositional estimates. All images were collected at an accelerating voltage of 10 kV. Beam currents ranged from about 275 pA for higher resolution images to about 5 nA for EDS acquisitions.

Raman spectra of SWCNTs were recorded using an excitation wavelength of 532 nm on a LabRam instrument from Jobin Yvon Horiba equipped with an Olympus confocal microscope. Generally, the laser beam was focused on the sample with a 50× microscope objective (laser spot size ≈ 1–2 μm). An exposure time of 15 s with three spectra accumulations was used on as-synthesized SWCNT samples. A shorter exposure time was used on purified SWCNTs to avoid Raman signal saturation. As-synthesized SWCNT samples were first ground into a homogeneous powder and then pressed into thin wafers. Purified SWCNTs were measured directly on carbon films coated on 0.4 μm pore nylon filters after filtration. Raman spectra were acquired from five randomly selected spots to confirm the sample homogeneity and the reproducibility of the spectra.

The quality of SWCNTs was also evaluated by UV–vis−NIR spectroscopy modified from the method proposed by Haddon *et al.*[40] Ten milligram samples of different SWCNTs were suspended in 20 mL of 1% sodium dodecyl benzenesulfonate (SDBS)/D_2O (99.9 atom % D, Sigma-Aldrich) solution and sonicated using a cup-horn ultrasonicator (SONICS, VCX-130) at 20 W for 30 min. After ultrasonication, the suspension was centrifuged for 1 h at *ca.* 53000*g* to obtain a stable and semitransparent SWCNT dispersion. The UV–vis−NIR absorption spectra were measured on a Varian Cary 5000 UV–vis−NIR spectrophotometer. The (*n*,*m*) distribution of SWCNTs was monitored using a fluorescence spectrometer. Fluorescence spectroscopy measurements were conducted on a Jobin-Yvon Nanolog-3 spectrofluorometer equipped with an InGaAs near-infrared detector.

Purified SWCNTs were processed to be separated by chirality. About 1 mg of single-stranded DNA $d(GT)_{30}$ mixed with 1 mg of the purified SWCNTs was sonicated for 120 min at a power of 8 W to yield 0.2–0.4 mg/mL DNA−SWCNT solution. Insoluble materials were removed by centrifugation, which also removed any remaining metal particles present.[27] Different fractions from anion exchange chromatography separation were analyzed by UV–vis−NIR spectroscopy. In order to probe the defect level in SWCNT samples, a (6,5)-enriched fraction was studied in redox titration. For comparison, the (6,5)-enriched fraction was also obtained in a similar way from commercially available CoMoCAT SWCNTs. Redox titration on the two different (6,5) samples using $KIrCl_6$ was carried out according to the published procedure.[27] For quantitative comparison, the concentration of each sample was adjusted so that the optical density at 990 nm, the E_{11} transition of the (6,5) tubes, is 1 for both samples.

The purified SWCNTs were also dispersed by sonication in dichloroethane and then spread on a substrate with predefined electrodes. FET characteristics were measured following a procedure described elsewhere.[28]

Acknowledgment. The authors are grateful to U.S. Department of Energy, Office of Basic Energy Sciences, Grant No. DE-FG02-01ER15183. This project is also supported by the Nanyang Technological University CoE-SUG and AcRF grant RG 38/06 and RG 106/06.

Supporting Information Available: EDS data for composition analysis of purified SWCNT samples. This material is available free of charge *via* the Internet at http://pubs.acs.org.

REFERENCES AND NOTES

1. Dresselhaus, M. S.; Dresselhaus, G.; Eklund, P. C. *Science of Fullerenes and Carbon Nanotubes*; Academic Press: San Diego, 1996; p 985.
2. Dresselhaus, M. S. Nanotubes: A Step in Synthesis. *Nat. Mater.* **2004**, *3*, 665–666.
3. Sen, R.; Rickard, S. M.; Itkis, M. E.; Haddon, R. C. Controlled Purification of Single-Walled Carbon Nanotube Films by Use of Selective Oxidation and Near-IR Spectroscopy. *Chem. Mater.* **2003**, *15*, 4273–4279.
4. Valentini, F.; Amine, A.; Orlanducci, S.; Terranova, M. L.; Palleschi, G. Carbon Nanotube Purification: Preparation and Characterization of Carbon Nanotube Paste Electrodes. *Anal. Chem.* **2003**, *75*, 5413–5421.
5. Gregan, E.; Keogh, S. M.; Maguire, A.; Hedderman, T. G.; Neill, L. O.; Chambers, G.; Byrne, H. J. Purification and Isolation of SWNTs. *Carbon* **2004**, *42*, 1031–1035.
6. Bendjemil, B.; Borowiak-Palen, E.; Graff, A.; Pichler, T.; Guerioune, M.; Fink, J.; Knupfer, M. Elimination of Metal Catalyst and Carbon-Like Impurities from Single-Wall Carbon Nanotube Raw Material. *Appl. Phys. A: Mater. Sci. Process.* **2004**, *A78*, 311–314.
7. Fang, H.-T.; Liu, C.-G.; Liu, C.; Li, F.; Liu, M.; Cheng, H.-M. Purification of Single-Wall Carbon Nanotubes by Electrochemical Oxidation. *Chem. Mater.* **2004**, *16*, 5744–5750.
8. Haddon, R. C.; Sippel, J.; Rinzler, A. G.; Papadimitrakopoulos, F. Purification and Separation of Carbon Nanotubes. *MRS Bull.* **2004**, *29*, 252–259.
9. Lian, Y.; Maeda, Y.; Wakahara, T.; Akasaka, T.; Kazaoui, S.; Minami, N.; Shimizu, T.; Choi, N.; Tokumoto, H. Nondestructive and High-Recovery-Yield Purification of Single-Walled Carbon Nanotubes by Chemical Functionalization. *J. Phys. Chem. B* **2004**, *108*, 8848–8854.
10. Vivekchand, S. R. C.; Govindaraj, A.; Seikh, M. M.; Rao, C. N. R. New Method of Purification of Carbon Nanotubes Based on Hydrogen Treatment. *J. Phys. Chem. B* **2004**, *108*, 6935–6937.
11. Nepal, D.; Kim, D. S.; Geckeler, K. E. A Facile and Rapid Purification Method for Single-Walled Carbon Nanotubes. *Carbon* **2005**, *43*, 660–662.
12. Rinzler, A. G.; Liu, J.; Dai, H.; Nikolaev, P.; Huffman, C. B.; Rodriguez-Macias, F. J.; Boul, P. J.; Lu, A. H.; Heymann, D.; Colbert, D. T.; *et al.* Large-Scale Purification of Single-wall Carbon Nanotubes: Process, Product, and Characterization. *Appl. Phys. A: Mater. Sci. Process.* **1998**, *67*, 29–37.
13. Liu, J.; Rinzler, A. G.; Dai, H.; Hafner, J. H.; Bradley, R. K.; Boul, P. J.; Lu, A.; Iverson, T.; Shelimov, K.; Huffman, C. B.; et al. Fullerene Pipes. *Science (Washington, D.C.)* **1998**, *280*, 1253–1256.
14. Chattopadhyay, D.; Galeska, I.; Papadimitrakopoulos, F. Complete Elimination of Metal Catalysts from Single Wall Carbon Nanotubes. *Carbon* **2002**, *40*, 985–988.
15. Igarashi, H.; Murakami, H.; Murakami, Y.; Maruyama, S.; Nakashima, N. Purification and Characterization of Zeolite-Supported Single-Walled Carbon Nanotubes Catalytically Synthesized from Ethanol. *Chem. Phys. Lett.* **2004**, *392*, 529–532.

16. Dillon, A. C.; Gennett, T.; Jones, K. M.; Alleman, J. L.; Parilla, P. A.; Heben, M. J. A Simple and Complete Purification of Single-Walled Carbon Nanotube Materials. *Adv. Mater. (Weinheim, Ger.)* **1999**, *11*, 1354–1358.
17. Chiang, I. W.; Brinson, B. E.; Smalley, R. E.; Margrave, J. L.; Hauge, R. H. Purification and Characterization of Single-Wall Carbon Nanotubes. *J. Phys. Chem. B* **2001**, *105*, 1157–1161.
18. Kitiyanan, B.; Alvarez, W. E.; Harwell, J. H.; Resasco, D. E. Controlled Production of Single-Wall Carbon Nanotubes by Catalytic Decomposition of CO on Bimetallic Co-Mo Catalysts. *Chem. Phys. Lett.* **2000**, *317*, 497–503.
19. Lim, S.; Ciuparu, D.; Pak, C.; Dobek, F.; Chen, Y.; Harding, D.; Pfefferle, L.; Haller, G. Synthesis and Characterization of Highly Ordered Co-MCM-41 for Production of Aligned Single Walled Carbon Nanotubes (SWNT). *J. Phys. Chem. B* **2003**, *107*, 11048–11056.
20. Ciuparu, D.; Chen, Y.; Lim, S.; Haller, G. L.; Pfefferle, L. Uniform-Diameter Single-Walled Carbon Nanotubes Catalytically Grown in Cobalt-Incorporated MCM-41. *J. Phys. Chem. B* **2004**, *108*, 503–507.
21. Chen, Y.; Ciuparu, D.; Lim, S.; Yang, Y.; Haller, G. L.; Pfefferle, L. Synthesis of Uniform Diameter Single-Wall Carbon Nanotubes in Co-MCM-41: Effects of the Catalyst Prereduction and Nanotube Growth Temperatures. *J. Catal.* **2004**, *225*, 453–465.
22. Chen, Y.; Ciuparu, D.; Lim, S.; Yang, Y.; Haller, G. L.; Pfefferle, L. Synthesis of Uniform Diameter Single Wall Carbon Nanotubes in Co-MCM-41: Effects of CO Pressure and Reaction Time. *J. Catal.* **2004**, *226*, 351–362.
23. Luo, Z. T.; Pfefferle, L. D.; Haller, G. L.; Papadimitrakopoulos, F. (*n*,*m*) Abundance Evaluation of Single-Walled Carbon Nanotubes by Fluorescence and Absorption Spectroscopy. *J. Am. Chem. Soc.* **2006**, *128*, 15511–15516.
24. Lim, S.; Ciuparu, D.; Chen, Y.; Yang, Y.; Pfefferle, L.; Haller, G. L. Pore Curvature Effect on the Stability of Co-MCM-41 and the Formation of Size-Controllable Subnanometer Co Clusters. *J. Phys. Chem. B* **2005**, *109*, 2285–2294.
25. Zheng, M.; Jagota, A.; Strano, M. S.; Santos, A. P.; Barone, P.; Chou, S. G.; Diner, B. A.; Dresselhaus, M. S.; McLean, R. S.; Onoa, G. B.; *et al.* Structure-Based Carbon Nanotube Sorting by Sequence-Dependent DNA Assembly. *Science (Washington, D.C.)* **2003**, *302*, 1545–1548.
26. Zheng, M.; Jagota, A.; Semke, E. D.; Diner, B. A.; McLean, R. S.; Lustig, S. R.; Richardson, R. E.; Tassi, N. G. DNA-Assisted Dispersion and Separation of Carbon Nanotubes. *Nat. Mater.* **2003**, *2*, 338–342.
27. Zheng, M.; Diner, B. A. Solution Redox Chemistry of Carbon Nanotubes. *J. Am. Chem. Soc.* **2004**, *126*, 15490–15494.
28. Klinke, C.; Chen, J.; Afzali, A.; Avouris, P. Charge Transfer Induced Polarity Switching in Carbon Nanotube Transistors. *Nano Lett.* **2005**, *5*, 555–558.
29. Jorio, A.; Saito, R.; Dresselhaus, G.; Dresselhaus, M. S. Determination of Nanotubes Properties by Raman Spectroscopy. *Philos. Trans. R. Soc. London, Ser. A* **2004**, *362*, 2311–2336.
30. Jiang, C.; Kempa, K.; Zhao, J.; Schlecht, U.; Kolb, U.; Basche, T.; Burghard, M.; Mews, A. Strong Enhancement of the Breit-Wigner-Fano Raman Line in Carbon Nanotube Bundles Caused by Plasmon Band Formation. *Phys. Rev. B: Condens. Matter Mater. Phys.* **2002**, *66*, 161404/1161404/4.
31. Lim, S.; Ciuparu, D.; Chen, Y.; Pfefferle, L.; Haller, G. L. Effect of Co-MCM-41 Conversion to Cobalt Silicate for Catalytic Growth of Single Wall Carbon Nanotubes. *J. Phys. Chem. B* **2004**, *108*, 20095–20101.
32. Ferrari, A. C.; Robertson, J. Interpretation of Raman Spectra of Disordered and Amorphous Carbon. *Phys. Rev. B: Condens. Matter Mater. Phys.* **2000**, *61*, 14095–14107.
33. Shen, K.; Curran, S.; Xu, H.; Rogelj, S.; Jiang, Y.; Dewald, J.; Pietrass, T. Single-Walled Carbon Nanotube Purification, Pelletization, and Surfactant-Assisted Dispersion: A Combined TEM and Resonant Micro-Raman Spectroscopy Study. *J. Phys. Chem. B* **2005**, *109*, 4455–4463.
34. Chen, Y.; Ciuparu, D.; Lim, S.; Haller, G. L.; Pfefferle, L. D. The Effect of the Cobalt Loading on the Growth of Single Wall Carbon Nanotubes by CO Disproportionation on Co-MCM-41 Catalysts. *Carbon* **2006**, *44*, 67–78.
35. Ciuparu, D.; Chen, Y.; Lim, S.; Yang, Y.; Haller, G. L.; Pfefferle, L. Mechanism of Cobalt Cluster Size Control in Co-MCM-41 during Single-Wall Carbon Nanotubes Synthesis by CO Disproportionation. *J. Phys. Chem. B* **2004**, *108*, 15565–15571.
36. Haider, P.; Chen, Y.; Lim, S.; Haller, G. L.; Pfefferle, L.; Ciuparu, D. Application of the Generalized 2D Correlation Analysis to Dynamic Near-Edge X-ray Absorption Spectroscopy Data. *J. Am. Chem. Soc.* **2005**, *127*, 1906–1912.
37. Brown, S. D. M.; Jorio, A.; Corio, P.; Dresselhaus, M. S.; Dresselhaus, G.; Saito, R.; Kneipp, K. Origin of the Breit-Wigner-Fano Lineshape of the Tangential G-Band Feature of Metallic Carbon Nanotubes. *Phys. Rev. B: Condens. Matter Mater. Phys.* **2001**, *63*, 155414/1155414/8.
38. Kempa, K. Gapless Plasmons in Carbon Nanotubes and Their Interactions with Phonons. *Phys. Rev. B: Condens. Matter Mater. Phys.* **2002**, *66*, 195406/1195406/5.
39. Strano, M. S.; Huffman, C. B.; Moore, V. C.; O'Connell, M. J.; Haroz, E. H.; Hubbard, J.; Miller, M.; Rialon, K.; Kittrell, C.; Ramesh, S.; *et al.* Reversible, Band-Gap-Selective Protonation of Single-Walled Carbon Nanotubes in Solution. *J. Phys. Chem. B* **2003**, *107*, 6979–6985.
40. Itkis, M. E.; Perea, D. E.; Jung, R.; Niyogi, S.; Haddon, R. C. Comparison of Analytical Techniques for Purity Evaluation of Single-Walled Carbon Nanotubes. *J. Am. Chem. Soc.* **2005**, *127*, 3439–3448.
41. Krupke, R.; Hennrich, F.; Hampe, O.; Kappes, M. M. Near-Infrared Absorbance of Single-Walled Carbon Nanotubes Dispersed in Dimethylformamide. *J. Phys. Chem. B* **2003**, *107*, 5667–5669.
42. Minami, N.; Kazaoui, S.; Jacquemin, R.; Yamawaki, H.; Aoki, K.; Kataura, H.; Achiba, Y. Optical Properties of Semiconducting and Metallic Single Wall Carbon Nanotubes: Effects of Doping and High Pressure. *Synth. Met.* **2001**, *116*, 405–409.
43. Itkis, M. E.; Perea, D. E.; Niyogi, S.; Rickard, S. M.; Hamon, M. A.; Hu, H.; Zhao, B.; Haddon, R. C. Purity Evaluation of As-Prepared Single-Walled Carbon Nanotube Soot by Use of Solution-Phase Near-IR Spectroscopy. *Nano Lett.* **2003**, *3*, 309–314.
44. O'Connell, M. J.; Bachilo, S. M.; Huffman, C. B.; Moore, V. C.; Strano, M. S.; Haroz, E. H.; Rialon, K. L.; Boul, P. J.; Noon, W. H.; Kittrell, C.; *et al.* Band Gap Fluorescence from Individual Single-Walled Carbon Nanotubes. *Science (Washington, D.C.)* **2002**, *297*, 593–596.
45. Bachilo, S. M.; Strano, M. S.; Kittrell, C.; Hauge, R. H.; Smalley, R. E.; Weisman, R. B. Structure-Assigned Optical Spectra of Single-Walled Carbon Nanotubes. *Science (Washington, D.C.)* **2002**, *298*, 2361–2366.
46. Weisman, R. B.; Bachilo, S. M. Dependence of Optical Transition Energies on Structure for Single-Walled Carbon Nanotubes in Aqueous Suspension: An Empirical Kataura Plot. *Nano Lett.* **2003**, *3*, 1235–1238.
47. Martel, R.; Schmidt, T.; Shea, H. R.; Hertel, T.; Avouris, P. Single- and Multi-Wall Carbon Nanotube Field-Effect Transistors. *Appl. Phys. Lett.* **1998**, *73*, 2447–2449.
48. Kim, W.; Javey, A.; Vermesh, O.; Wang, Q.; Li, Y.; Dai, H. Hysteresis Caused by Water Molecules in Carbon Nanotube Field-Effect Transistors. *Nano Lett.* **2003**, *3*, 193–198.
49. Lim, S.; Yang, Y.; Ciuparu, D.; Wang, C.; Chen, Y.; Pfefferle, L.; Haller, G. L. The Effect of Synthesis Solution pH on the Physicochemical Properties of Co Substituted MCM-41. *Top. Catal.* **2005**, *34*, 31–40.
50. Barrett, E. P.; Joyner, L. G.; Halenda, P. P. The Determination of Pore Volume and Area Distributions in Porous Substances. 1. Computations from Nitrogen Isotherms. *J. Am. Chem. Soc.* **1951**, *73*, 373–380.